INTERNATIONAL JOURNAL FOR NUMERICAL AND ANALYTICAL METHODS IN GEOMECHANICS
Int. J. Numer. Anal. Meth. Geomech., **23**, 23–44 (1999)

COMPUTATIONAL MODEL FOR THE SIMULATION OF THE SHIELD TUNNELING PROCESS IN COHESIVE SOILS

MURAD Y. ABU-FARSAKH[†], AND GEORGE Z. VOYIADJIS*[‡]

Louisiana State University, Baton Rouge, LA 70803 U.S.A

SUMMARY

A two-dimensional computational model is developed here in order to simulate the continuous advance of the Earth Pressure Balance (EPB) Shield during the tunneling process in cohesive soils. The model is based on the combination of the plane strain "transverse–longitudinal" sections that can incorporate the three-dimensional deformation of the soil around and ahead of the shield face. This model is capable of prediciting the soil response due to the shield tunneling before the event, especially in soft ground conditions. An elasto-plastic finite element analysis that is based on the coupled theory of mixtures for inelastic porous media for finite deformation is used in this work to describe the time-dependent deformation of the saturated cohesive soils.[1] The results of this model are compared with the *in situ* field measurements of the N-2 tunnel project excavated in 1981 in San Francisco using the EPB shield tunneling machine. Reasonable agreement is found between the observed field measurements and the predicted deformations of the soil using the proposed numerical simulation. Copyright © 1999 John Wiley & Sons, Ltd.

Key words: tunneling; deformations; numerical modeling; soft ground

1. INTRODUCTION

Rapid growth in urban development has resulted in increasing the necessity for using underground space due to the need of upgrading and expanding the existing infrastructure in order to satisfy the updating demands. Tunneling will provide the necessary infrastructure and accommodation for future needs that minimize the surface impacts. Tunnels are essential in major cities in order to accommodate transportation systems, communication, and utility networks such as water supply and sewage disposal pipelines.

The development of the shield tunnel methods throughout the history has been concentrated on how to stabilize and support the cutting face during excavation. The cutting face during excavation can be supported by different ways such as mechanical means, compressed air, fluid, and by the excavated soil itself. The mechanical support is not suitable and very risky in soft

[†]Research Associate, Louisiana Transportation Research Center, LTRC, Baton Rouge, LA 70808, USA
[‡]Boyd Professor, Department of Civil and Environmental Engineering, Baton Rouge, LA 70803 U.S.A.

*Correspondence to: G. Z. Voyiadjis, Louisiana State University, Baton Rouge, LA 70803 U.S.A.

Contract grant sponsor: National Science Foundation; contract grant number MSS-9312707

CCC 0363–9061/99/010023–22$17.50

Received 20 May 1997
Revised 18 February 1998

ground especially below groundwater level.[2] The compressed air shield was the first approach used in soft ground. The slurry shield system followed after that where the face is supported by a fluid (usually water and additives such as bentonite). In 1974, the Earth Pressure Balance (EPB) shield system was introduced in Japan, in which the excavated soil material itself supports the cutting face. The pressure applied to the tunnel face counterbalances, in theory, the existing overburden and hydrostatic pressures. The EPB shield was first used in the U.S.A in 1981 to drive a 3·7 m diameter, 915 m long tunnel for the San Francisco clean water project.

Recent advances in the tunneling technology help in reducing the construction time with the decrease in the cost. Unfortunately, theoretical advances have not kept pace with the recent advances in the tunneling technology. Construction of tunnels in soft ground, especially in urban regions, poses a unique challenge to engineers, and careful consideration must be given to the magnitude and distribution of settlements. At present there is no general method for predicting the ground subsidence owing to tunneling before the tunnel construction. Up to date empirical procedures (e.g. Reference 3) have been widely used, to predict the ground deformation owing to tunneling. Nevertheless, empirical formulas have limitations in their applicability to different tunnel geometries, different construction techniques, different soil conditions.[4] It has been reported that deformation caused by tunneling[5] and the subsequent potential damage to adjacent and overlying services and structures depends on the ground and groundwater condition, tunnel depth and geometry, and the construction procedure which is the most important factor.

Recently, the prediction of ground deformation and stress patterns during shield tunneling has been carried out by numerical analysis based on the finite element methods. Due to simplicity and cost effectiveness, in many cases, researchers (e.g. References 5–9) adapted the two-dimensional plane strain or axi-symmetrical approach of the tunnel transverse or longitudinal section. However, field results and theoretical analyses show that the general stress and displacement patterns around the tunnel are three-dimensional and different from the plane strain transverse section.[10,11] During the shield advance, before the face of the tunnel shield reaches the section, the soil is subjected to small settlement or heave movement. As the tunnel shield passes the section, a rapid downward settlement of the soil occurs immediately after the tailpiece cleared the section invading the space (gap) between the tunnel boundary and the lining. At this stage, the lined tunnel section approaches the plane strain condition. The distance required for ground displacement to reach the plane strain condition depends on the amount of plasticity developed around the tunnel. Under idealized construction, when the tunneling machine is kept hard against the face minimizing the stress changes and deformation into the face, the tunnel is advanced under perfect alignment and can be treated as a plane strain case. Under a less conservative construction procedure, the three-dimensional movement ahead of the tunnel face may be significant. Construction difficulties such as steering and alignment problems, can cause over excavation and remolding of adjacent soils. Usually, during tunneling, a significant disturbed zone is induced around the tunnel. Several attempts have been made to use 3-D finite element model[10–14] to simulate the tunneling process especially for open face tunneling shields. Akagi[14] used excavated elements ahead of the shield face to simulate the advance of the shield in the 3-D model. Finno and Clough[8] introduced a 2-D model that is based on the combination of both the transverse and longitudinal plane sections. The longitudinal section analysis used to provide information of the nature of the pressure distribution in order to stimulate the heaving process in the transverse section.

In this work, a two-dimensional computational model is developed and used to simulate the continuous advance of the Earth Pressure Balance (EPB) Shield during the tunneling process in

cohesive soils. The model is based on the plane strain 'transverse–longitudinal' sections that is capable of simulating the continuous advance of the shield and incorporating the 3-D deformation of the soil around and ahead of the shield face. The remeshing technique is used in the longitudinal section to rearrange the finite element mesh ahead of the shield face so that the size and dimension of the excavated elements match the geometric shape and size of the shield advance. An elastoplastic coupled equations that is based on the theory of mixtures for inelastic porous media for finite deformation[1,15] is used in this work to describe the time-dependent deformation of the saturated cohesive soils. The computational model is used to analyse the N-2 tunnel project excavated in 1981 in San Francisco using the EPB shield tunnel machine. The results of this analysis are compared with the *in situ* field measurements of the N-2 tunnel project.

2. FINITE ELEMENT FORMULATION

An elastoplastic coupled system of equations is used in this work to describe the time-department deformation of the saturated cohesive soils. Formulation of these equations is based on the principle of virtual work and the theory of mixtures for inelastic porous media. The coupled equations are developed for large deformations with finite strains using the updated Lagrangian formulation in order to incorporate the geometric non-linearities of the soil. The detailed description of the formulation of the coupled equations has been presented elsewhere.[1] Here a brief description is presented.

In the updated Lagrangian formulation, the reference configuration is updated after each incremental step. The relation between the co-ordinates at $n+1$ (X_i^{n+1}) and n configurations (X_i^n) is given by the following equation:

$$X_i^{n+1} = X_i^n + \Delta u_i \tag{1}$$

where Δu_i is the incremental displacement.

For finite deformations, the elastoplastic constitutive equation for the solid skeleton is assumed to be

$$\mathring{\sigma}'^{\mathrm{s}}_{ab} = D^{\mathrm{s}}_{abcd}\, d^{\mathrm{s}}_{cd} \tag{2}$$

where D^{s} is the elastoplastic stiffness matrix. $\mathring{\sigma}'^{\mathrm{s}}$ is the Jaumann effective stress rate tensor given as

$$\mathring{\sigma}'^{\mathrm{s}}_{ij} = \mathring{\sigma}'^{\mathrm{s}}_{ij} - w^{\mathrm{s}}_{ik}\sigma'^{\mathrm{s}}_{kj} + w^{\mathrm{s}}_{kj}\sigma'^{\mathrm{s}}_{ik} \tag{3}$$

where $\mathring{\sigma}'^{\mathrm{s}}$ is the effective Cauchy stress rate tensor, $\mathring{\sigma}'^{\mathrm{s}}$ is the effective Cauchy stress tensor, $\mathbf{d}^{\mathrm{s}}$ is the deformation rate given by

$$\mathrm{d}^{\mathrm{s}}_{ij} = \tfrac{1}{2}(\mathbf{v}^{\mathrm{s}}_{i,j} + \mathbf{v}^{\mathrm{s}}_{j,i}) \tag{4}$$

and

$$W^{\mathrm{s}}_{ij} = \tfrac{1}{2}(\mathbf{v}^{\mathrm{s}}_{i,j} - \mathbf{v}^{\mathrm{s}}_{j,i}) \tag{5}$$

is the spin tensor. In equations (4) and (5), $\mathbf{v}^{\mathrm{s}}$ is the velocity of the solid particles.

The incremental stress–strain relationship is given as follows:[1,15]

$$\Delta S_{ij} = D^{*}_{ijkl}\Delta\varepsilon_{kl} + J^{\mathrm{s}}X^{\mathrm{s}}_{I,i}\,X^{\mathrm{s}}_{J,j}\,\delta_{ij}\Delta P_w \tag{6}$$

where $\Delta\mathbf{s}$ is the incremental second-Piola Kirkchoff, $\Delta\varepsilon$ is the material incremental strain tensor, $\mathbf{D}^*$ is the modified elastoplastic stiffness matrix[1,15] ΔP_w is the incremental pore water pressure,

δ is the kronecher delta, J^s is the Jaccobian of the solid grains, and $\mathbf{x}^s$ is the deformation gradient for the solid grains given by

$$X^s_{I,i} = \frac{\partial^{n+1} X^s_I}{\partial^n X^s_i} \tag{7}$$

Using the finite element discretization, the incremental strains can be expressed as follows:

$$\delta\varepsilon = (\mathbf{B}_L + \mathbf{B}_{NL})\delta U_d \tag{8}$$

where B_L and B_{NL} are the linear and non-linear strain–displacement matrices.

The complete coupled behaviour of the two-phase soil-fluid state can be expressed as follows:[1, 15]

$$\begin{bmatrix} {}_n\mathbf{K} & -{}_n\Omega \\ -{}_n\Omega^T & -\delta t\,{}_n\Psi \end{bmatrix} \begin{Bmatrix} \Delta\mathbf{U}_d \\ \Delta\mathbf{U}_p \end{Bmatrix} = \begin{Bmatrix} {}_n\Phi \\ {}_n\Pi \end{Bmatrix} \tag{9}$$

where ${}_n\mathbf{K} = {}_n\mathbf{K}_L + {}_n\mathbf{K}_{NL} + {}_n\mathbf{K}^T_{NL} + {}_n\mathbf{K}^G$ is the stiffness matrix, ${}_n\mathbf{K}_L$, ${}_n\mathbf{K}_{NL}$, ${}_n\mathbf{K}^G$ are the linear, non-linear and geometric non-linear stiffness matrices respectively; ${}_n\Omega$ is the coupling matrix, ${}_n\Psi$ is the flow matrix, $\Delta\mathbf{U}_d$ is the incremental nodal displacements, and ΔU_p is the incremental nodal excess pore pressures.

The coupled system of equations are implemented into a finite element program (GAP/CTM). The upper triangular matrix up to the sky line is only stored in this program. Transformation is done at the end of each incremental step in order to obtain the current updated deformed configuration and to update all variables (displacements, stresses and strains) to be used for the next increment. The Newton–Raphson iterative technique is used here to obtain the converged solution within each increment.

3. FINITE ELEMENT NUMERICAL SIMULATION

The continuous advance of the tunneling process is simulated here by using the two-dimensional finite element analysis that is based on the combination of both the plane strain 'longitudinal and transverse' sections. The plane strain longitudinal section will be used to simulate the continuous advance of the shield and to study the short-term soil deformation, stress redistribution and excess pore pressure ahead of shield. The analysis of the longitudinal section will provide us with important information that is needed in the transverse analysis such as the initial surface heave or settlement and the distribution of the excess pore pressure around the tunnel opening. Based on the results of the longitudinal section, a second analysis is done for the plane strain transverse section. The effect of the three-dimensional deformation is incorporated into the transverse section analysis. The plane strain transverse section analysis provides us with the complete information of the short-term, as well as, the long-term soil deformation, stress and strain changes around the tunnel opening, and the surface settlements with time.

3.1. 2-D longitudinal section

A 2-D longitudinal section is used to simulate the advancement of the EPB shield and the associated ground deformation and stresses redistribution resulting from the shield advancement. The advancement of the tunneling machine involves a change in geometry and removal of excavated soil, so that a step-by-step incremental excavation procedure will be used in this

simulation. The EPB shield machine can be operated in such a way that the rate of excavating of the soil is more, less or equal to the rate of advancing the shield thus causing over, under or perfect excavation simultaneously, by adjusting the applied earth pressure at the shield face. In most cases, the EPB shield is operated so that the rate of excavation is less than the rate of advancing the machine forcing the soil away from its face causing small initial heave. This initial heave will reduce the amount of final settlement. The magnitude of the heave is directly proportional to the applied earth pressure. However, the proposed model will be capable of handling the three mentioned cases and for both open and closed face shields. For overexcavation case, in each incremental advance, part of the soil will move inside the shield causing the incremental excavation to be higher than the incremental advance. For underexcavation case, in each incremental advance, part of the soil ahead of the face will be excavated and part will be displaced away of the shield face. For perfect excavation case, the soil is neither displaced away nor moved inside.

During the continuous advancement of the shield tunneling machine, soil elements ahead of the tunnel face usually undergo large deformations and hence change in geometry. Therefore, in order to avoid more/or less volume excavation, it is necessary to perform remeshing for the finite elements ahead of the shield face. This is done by arranging the finite element mesh ahead of the shield face so that the size and dimensions of the excavated elements for the next incremental step match the geometric shape and size of the incremental shield advance as shown in Figure 1.

In the longitudinal plane strain analysis, the simulation of the advancement of the EPB shield tunneling will be accomplished in the following three stages as described in Figure 2:

Stage 1: Removal of the part of the soil ahead the shield that has to be excavated and replace it with equivalent traction acting around the tunnel and move the face of the shield just ahead of the excavated part.

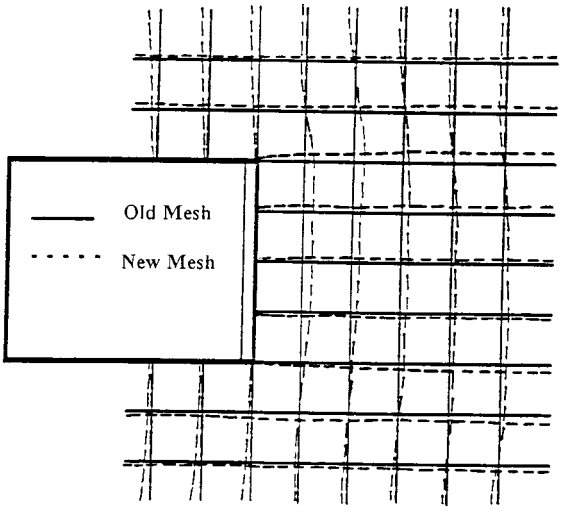

Figure 1. Remeshing of the finite elements ahead of the tunnel machine

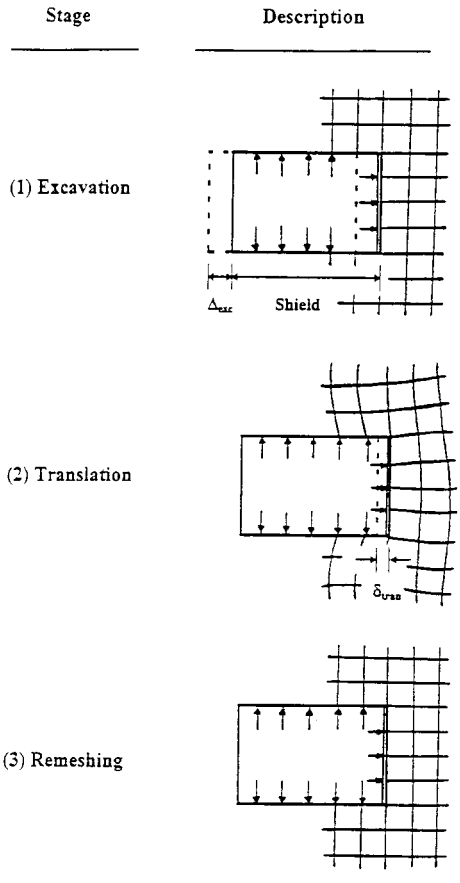

Figure 2. Stages of the two-dimensional longitudinal section

Stage 2:

Under excavation: Apply incremental rigid translations of the nodes representing the face and the body of the EPB shield until the average earth pressure at the face reaches the specified controlled value (based on the machine operation). This will simulate the initial heaving process caused by displacing the soil away from the face.

Over excavation: Gradually release the nodes representing the face of the EPB shield until the average earth pressure at the face reaches the specified controlled value. This will simulate the initial settlement process caused by inward movement of the soil into the shield chamber.

Perfect excavation: Disregard this stage.

Stage 3: *Remeshing*: The finite element mesh will be rearranged in the portion ahead of the shield face so that the size and dimensions of the excavated elements for the next incremental step match the geometric shape and size of the incremental shield advance (Figures 1 and 2(c)).

Stages 1–3 will be repeated for other excavation increments until a plane strain condition is reached just behind the shield tail, or to achieve a specified excavation distance. The strength and

the Poisson's ratio for the elements immediately ahead of the shield face will be reduced to represent the disturbed zone.

3.2. 2-D transverse section

In order to incorporate the three-dimensional deformation into the plane strain transverse section analysis, we need to find the magnitude and distribution of the radial heave/settlement pressure needed to be applied in the transverse section in order to simulate the initial heave/settlement stage. The results of the longitudinal section analysis will provide us with information about the distribution of the excess pore pressure and the stress change. In this analysis the distribution of the radial pressure is obtained by applying a rigid transition of the nodes representing the shield body and face in a simple 3-D model. The magnitude of the radial pressure is controlled by the excess pore pressure value at the springline. The radial pressure will be applied incrementally in the transverse section analysis until the excess pore pressure at the springline reaches the value obtained from the longitudinal section.

Simulation in the transverse plane strain section will be accomplished in the following five stages as described in Figure 3:

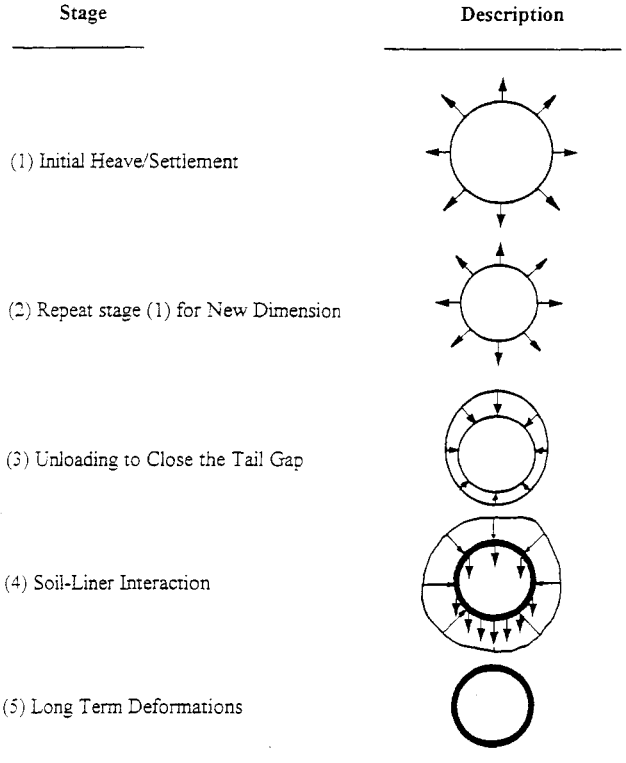

Figure 3. Two-dimensional transverse section simulation

Stage 1: Apply (or unload for initial settlement) incrementally the heave/or settlement pressure until the specified excess pore pressure at the springline is achieved (for perfect excavation, disregard this stage). In this stage, the peripheral nodal displacements can be estimated.

Stage 2: Knowing the peripheral nodal displacements, stage 1 is repeated with a new mesh using a different tunnel opening such that at the end of the heaving stage, the actual tunnel opening is reached.

Stage 3: Apply incremental unloading pressure around the tunnel periphery until the tail gap is closed (in case of grouting, unload until the grouting pressure is achieved). Nodes around the peripheral of the tunnel are allowed to move inward. The tail gap is considered closed when the relative movement of the node at the crown and at the invert equal the theoretical size of the tail gap. It is better to choose the distribution of the unloading pressure in such a way to insure the closure of the gap at the springline and at both the crown and the invert simultaneously. Reasonable results can be obtained from using a uniform unloading pressure distribution.

Stage 4: Once the soil comes into contact with the lining, the soil–lining interaction will be activated by changing the material properties of the inner element (must have the same size of the lining) in order to represent the actual lining material. In addition, the weight of the erected lining and the remaining of the peripheral pressure will be applied incrementally to the soil elements around the tunnel.

Stage 5: The time-dependent long-term deformation resulting from the dissipation of the developed excess pore pressure is simulated here.

3.3. Adaptive remeshing

During the tunneling process, the soil elements ahead and around the tunnel face undergo large deformations (even though there are low strains) causing changes in the elements geometry. Therefore, in order to avoid more/or less excavation due to the removal of the excavated soil elements, remeshing is done in the portion ahead of the shield face. This is done by rearranging the finite element mesh in the portion ahead of the shield face so that the size and dimensions of the excavated elements for the next incremental step match the geometric shape and size of the incremental shield advance (as shown in Figure 1).

The r-method will be used in this work to rearrange the finite element mesh in the portion ahead of the shield face. The idea is to relocate the node coordinates of the mesh so as to serve the mentioned goal. Since the number of nodes is unchanged during this adoption, therefore for computational efficiency, the r-method is considered for this case as the best among the other methods.[16]

3.3.1. Mapping of variables: In general the mapping process mainly consists of the following three essential steps:[17]

(1) Element identification (EI) to identify the element E_0 that contains the node n.
(2) Isoparametric inversion (IIN) to determine the isoparametric local coordinates (ξ^n, η^n) of the node n in the element E_0.
(3) Data transfer (DTR) to transfer data (values and variables) from element E_0 to the node n with local coordinates, (ξ^n, η^n).

(*I*) *Mapping of nodal variables* (*displacements and pore pressures*): For the node in the new mesh (α_{RM}) element (see Figure 4), one needs to first identify the element in the old mesh (α) that contains the node and hence determine the corresponding isoparametric local co-ordinates of that node using the modified Newton–Raphson iterative method.

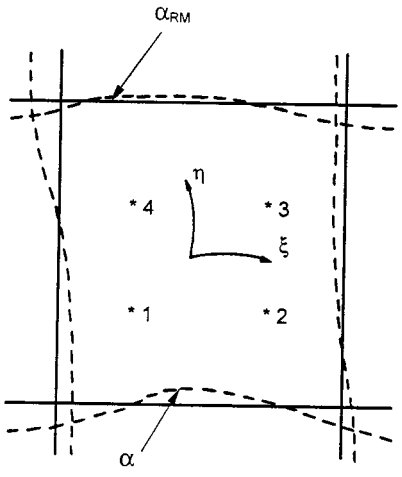

Figure 4. Rearrangement of the finite element mesh

To ensure that the node n lies inside the element E_0, the following constrains must be satisfied:

$$-1 \leqslant \xi^n \leqslant 1 \tag{10a}$$

$$-1 \leqslant \eta^n \leqslant 1 \tag{10b}$$

Once the local co-ordinates (ξ^n, η^n) are known, the nodal displacements and pore pressures can be interpolated from the E_0-nodes to node n using the interpolation functions N_k (may be taken of different interpolation functions used in the finite element analysis). If the node lies at the border between two or more elements (ξ^n or $\eta^n \sim 1$) and identified in more than one element, the nodal variables will be averaged.

(*II*) *Mapping of stresses and strains at Gauss points*: Since the mapping of stresses at the Gaussian element interpolation points (IPs) is done after each increment, the new IPs of the α_{RM} element will remain inside the α element. For mapping of stresses and strains from α_{RM} element to α element, the least square smoothing will be used for this purpose. The first step before smoothing is to obtain the isoparametric local co-ordinates of the new IPs with respect to the old element 'isoparametric inversion'. The modified Newton–Raphson iterative method is also used in order to obtain the local co-ordinates of the new IPs with respect to the α element.

Once the isoparametric local coordinates (ξ^n, η^n) are obtained for all the new IPs in the α_{RM} (with respect to the α_{RM} element), the least-squares smoothing of stresses and strains can be carried out over the whole finite element domain 'global smoothing' or performed separately over each individual element 'local smoothing'. The problem is then to find the set of smoothed stresses from the unsmoothed stresses that minimize the squares of errors using smoothing shape function (may be taken of different interpolation functions used in the finite element analysis).

(*III*) *Determination of the yield stress at the new Gauss points*: In the elastoplastic analysis, one needs to transfer the model's yield surface from the old IPs of the α element to the new IPs of the α_{RM} element. One way to do that is by interpolating or least-squares smoothing of the yield surface from old IPs to the new IPs. This can lead to values that are not self-consistent[17] (i.e. the effective stress σ' may be greater than the yield stress σ'_Y). Lee and Bathe[17] suggested that the yield

stress (σ'_Y) at the new IPs should be obtained from the mapped equivalent plastic strain and the strain hardening function as

$$\sigma'_Y = f(\varepsilon^p_{eq}) \tag{11}$$

The equivalent plastic strain can be mapped using the same method used to map stresses and strains.

4. ANALYSIS OF THE N-2 TUNNEL

The developed computational model is used to analyse the N-2 tunnel project excavated in San Francisco constructed in 1981. The soil condition of the N-2 tunnel site consists of an average of 6·1 m of rubble fill underlain by 9·1 m of soft sediment, known locally as Recent Bay Mud. A stratum of colluvium and residual sandy clay is encountered below the Bay Mud (complete description of the subsurface condition can be found in Reference 18). The tunnel of 3·7 m diameter is advanced within the Recent Bay Mud stratum. The fill is classified to be loose to medium dense. The recent Bay Mud consist mainly of silt and lean clay which is normally consolidated. The ground water table is located at 3 m below ground surface.

Figure 5 represents the finite element mesh used in the longitudinal section analysis; while Figure 6 represent the finite element mesh used in the transverse section analysis. The eight-noded isoparametric finite element, Q8P4, is used to represent the cohesive soil of the Recent Bay Mud. The Q8 element is used to represent the cohesionless soil of the fill and colluvium. The pore pressures are kept fixed at the bottom of the rubble fill and at the top of the colluvium. Six-noded thin-layer isoparametric interface slip elements (Q6P4) are arranged between the shield machine and the soil in order to model the soil-shield interface friction. The modified Cam clay model is used in this study in order to describe the plastic behaviour of normally consolidated cohesive soil. A non-linear hyperbolic model is used to describe the cohesionless soil response (fill and colluvium). An elasto-plastic constitutive frictional model of the Mohr–Coulomb type is used in

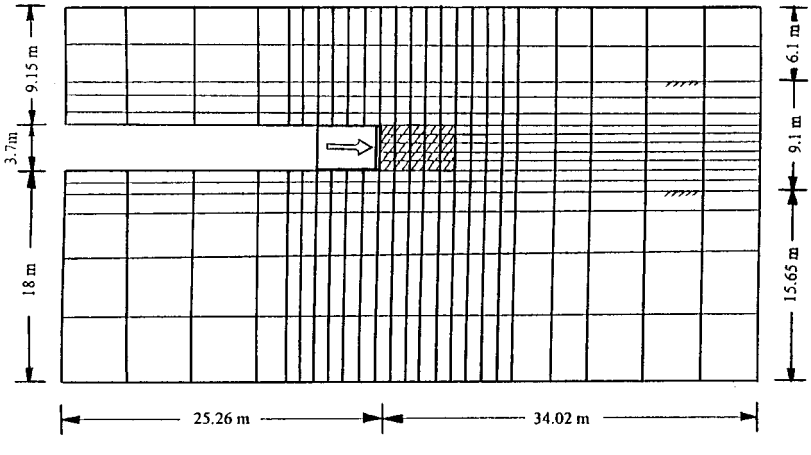

Figure 5. Finite element mesh for the longitudinal section analysis

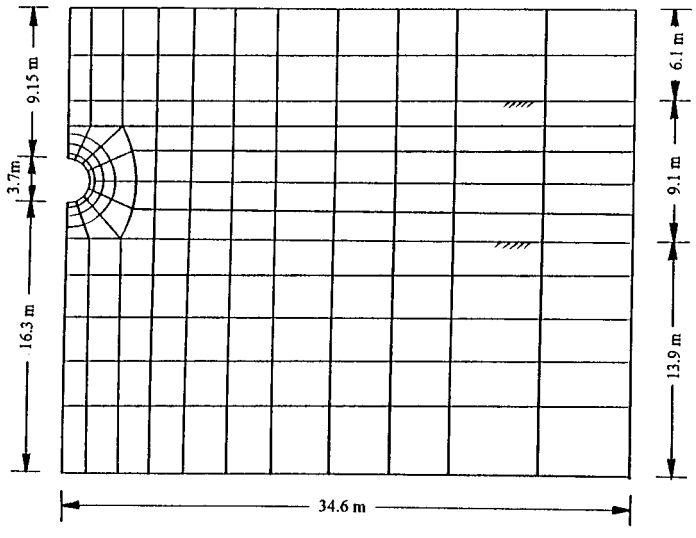

Figure 6. Finite element mesh for the transverse section analysis

Table I. Soil parameters for the non-linear hyperbolic model (after Finno and Clough, 1985)

Parameter	Fill	Colluvium
v, Poisson's ratio	0·3	0·35
R_f, failure ratio	0·9	0·9
ϕ, effective friction angle	30°	20°
C, cohesion, in kPa	14·36	47·88
n, modulus exponent	0·5	0·4
K, primary loading modulus constant	400	945
K_o, lateral earth pressure coefficient	0·5	0·8
γ_t, total unit weight, in kN/m^3	15·75	19·68

order to describe the response of the interface elements. The yield function of the Mohr–Coulomb type is given by

$$f \equiv \tau^2 - (C_a + \sigma'_n \tan\delta)^2 = 0 \tag{12}$$

where τ is the shear stress, σ'_n is the effective normal stress at the surface, C_a, is the adhesion, and δ is the interface friction angle and can be taken as $\delta = 2/3\phi$. ϕ is the angle of friction of the soil.

The soil parameters used in this analysis are taken from Finno and Clough.[18] Table I describes the soil parameters for the non-linear hyperbolic model used for the fill and colluvium stratas chosen from the test results for similar materials. The modified Cam-Clay soil parameters used for the Recent Bay Mud as presented in Table II are based on the isotropically consolidated undrained triaxial compression (CIU) tests.

In the longitudinal analysis, the average applied face pressure is kept at 74·25 kPa. The EPB shield is successfully advanced a distance equal to 1·5 times the shield length as illustrated in

Table II. Soil parameters for cam–clay model (after Finno and Clough, 1985)

Parameter	Recent Bay Mud
λ, slope of isotropic compression line	0·326
κ, slope of isotropic unloading-reloading line	0·043
M, slope of the critical state line	1·2
Void ratio at critical state and unit pressure	3·72
Ratio of shear modulus to effective overburden pressure	40
$kv; kh = 5\,kv$, coefficient of permeability, in m/s	10^{-8}
γ_t, total unit weight, in kN/m^3	16·53

Figure 5 by the dashed elements. This has been accomplished by five subsequent excavation steps. At each step of excavation, a rigid translation is applied to the nodes representing the shield face and body until the average applied earth pressure reaches the specified value (74·25 kPa). The strength of the soil is reduced by 20 per cent for the elements just ahead of the shield face in order to represent the disturbed (remolded) zone created ahead of the tunnel face.

The distribution of the heaving pressure in the transverse section is determined from the analysis of a simple 3-D with rigid translation of the shield face and body. An elliptical pressure distribution of the ratio 1 : 5 : 1 for the crown: springline: invert, respectively, is adapted in this analysis. The heaving process is completed when a certain criterion is reached. This criterion is taken by many researchers to be based on the field measurements. This criterion can be taken as when the observed (measured) field heave is reached[7] or until the lateral observed displacement is achieved.[8] This criterion assumes that one knows the field measurements before the analysis. The aim in this study is to predict the soil response before-the-event. At this time, the heaving process is considered completed when the predicted excess pore pressure at the springline during heaving in the transverse section reaches the predicted excess pore pressure from the longitudinal analysis. In this study, this assumption seems to be reasonable.

The distribution of the unloading pressure during the closure of the gap of 15 cm is taken as 1 : 1·5 : 1 for the crown: springline: invert respectively in order to ensure that the closure of the gap at the springline, invert and crown occurs simultaneously. This ratio is determined after attempting different ratios. If a uniform unloading pressure distribution is adapted, consideration must be given to the fact that closure of the gap around the tunnel opening may not occur simultaneously. This, for example, can be achieved by monitoring each of the peripheral nodes separately. Once any node closes the corresponding gap, that node will be prevented from further movements. The unloading will be continued until the whole peripheral nodes close the gap.

5. RESULTS OF ANALYSIS

5.1. Deformation of the longitudinal section

The predicted longitudinal displacements ahead of the shield that are obtained from the longitudinal section analysis of the shield advance are compared with field data measured at 1·2 and 5·5 m in front of the shield as shown in Figure 7. Most of the longitudinal displacement occurs in the Recent Bay Mud layer. Good agreement can be seen between the predicted and observed

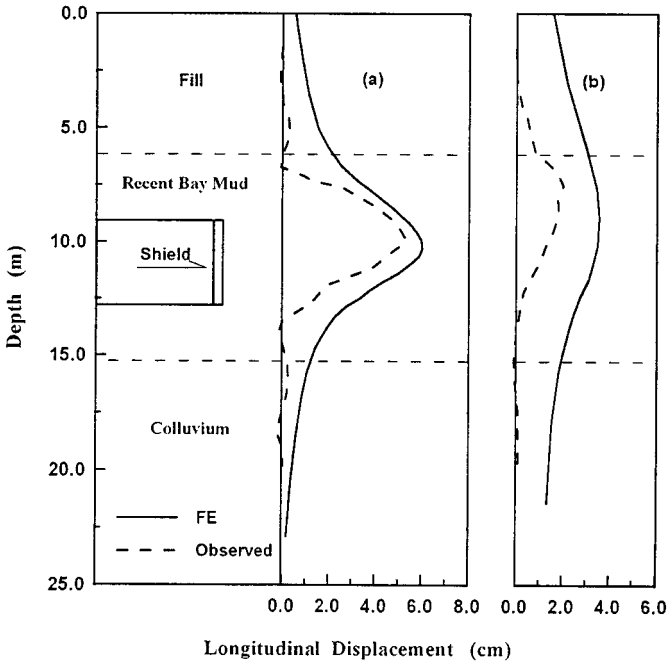

Figure 7. Longitudinal displacement ahead of the shield: (a) at 1·2 m ahead of the face; (b) at 5·5 m ahead of the face

longitudinal displacements at 1·2 m. However, the predicted displacements at 5·5 m are higher than the measured ones.

5.2. *Excess pore pressure and stress changes in the longitudinal section*

The contours of the predicted excess pore pressure in the Recent Bay Mud layer resulting from the shield advance in the longitudinal analysis are presented in Figure (8). The time required to advance the shield 7·5 m is estimated to be 0·82 days based on the average daily advancement (9·1 m/day). This time allows partial dissipation of the soil. The predicted excess pore pressure at the end of the shield advancement is 32·5 kPa immediately infront of the shield face and decreases rapidly with distance from the shield face.

Figures 9 and 10 represent the contours of axial stress change and shear stress respectively. The maximum predicted axial stress change of 21·8 kPa occurs around the bottom corner of the shield face. The predicted shear stress ranges from -16 kPa along the bottom of the shield body to 4–6 kPa along the top of the shield body. This is due to the fact that the effective normal stress is higher near the bottom of the shield.

5.3. *Deformations of the transverse section*

The predicted lateral deformation at the time of maximum heave is compared with the lateral measurements at a distance of 2·05 and 5·5 m from the tunnel centreline as shown in Figure 11.

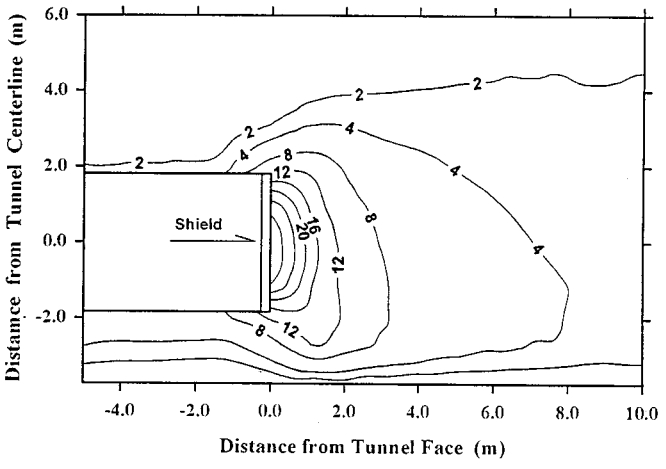

Figure 8. Contours of excess pore pressure (kPa)

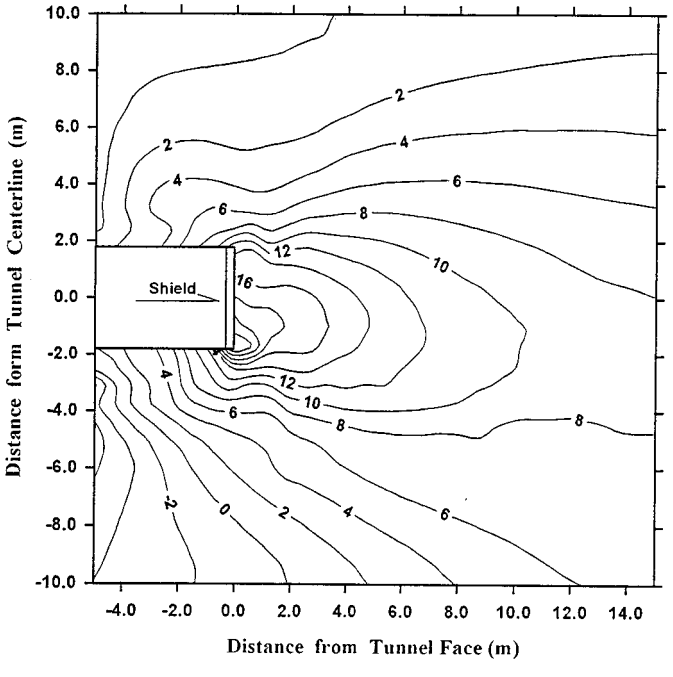

Figure 9. Contours of the axial stress change (kPa) at the longitudinal section

Good agreement is found between the predicted and observed lateral deformations. Both the observed and predicted deformations indicate that the maximum lateral deformation occurs slightly above the spring line, and most of the lateral deformation occurs in the Recent Bay Mud layer.

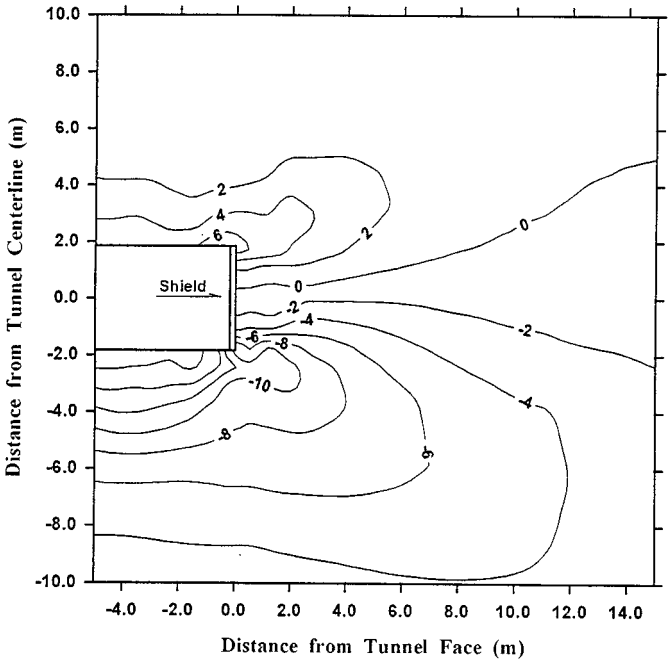

Figure 10. Contours of the shear stress (kPa) at the longitudinal section

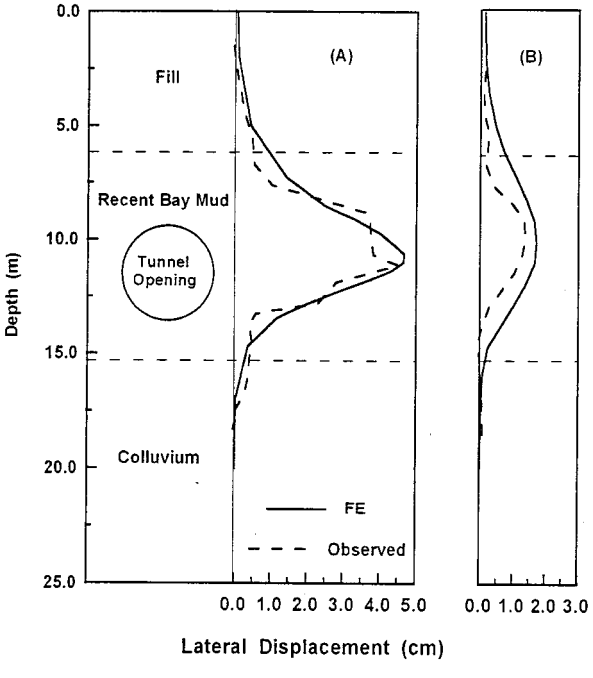

Figure 11. Lateral displacements at maximum Heave; (A) at 2·05 m from centreline; (B) at 5·5 m from centreline

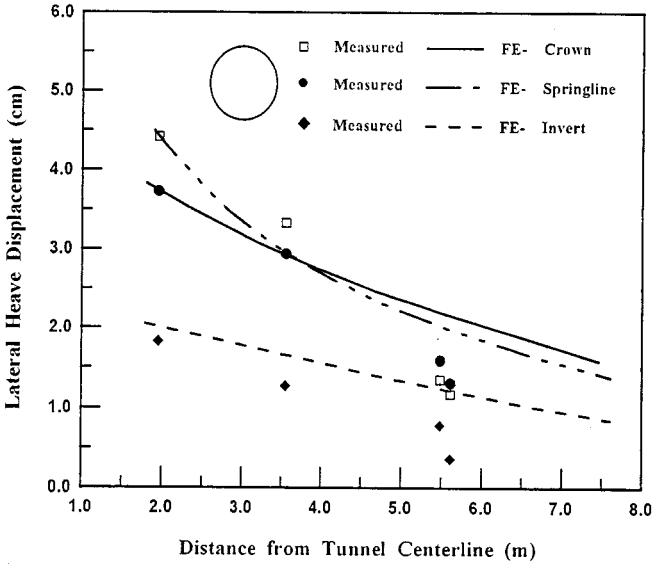

Figure 12. Predicted and observed lateral displacements distribution at maximum heave

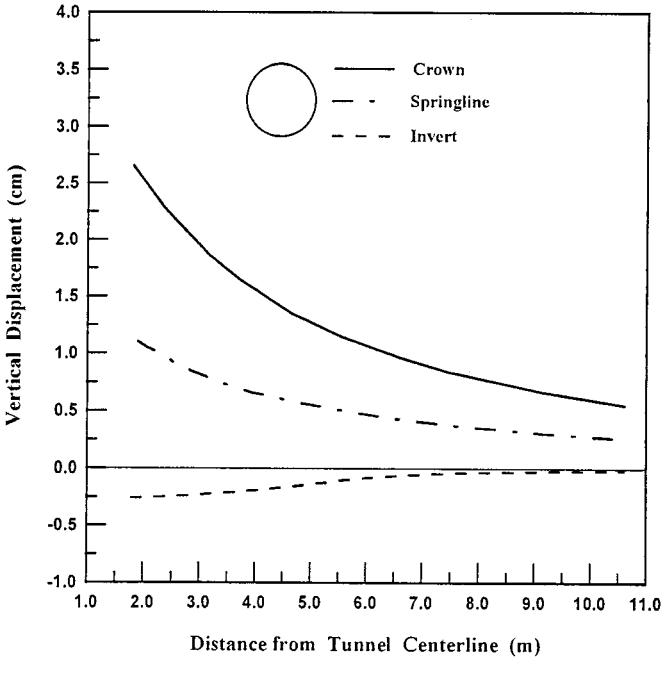

Figure 13. Predicted vertical displacements distribution at maximum heave

The predicted and observed lateral displacement distributions obtained at the time of maximum heave near the crown, springline and invert are shown in Figure 12. A good agreement with the field data can be seen for the distance less than 5 m from the tunnel centerline. Similarly, Figure 13 shows the distribution of the predicted vertical displacement obtained at the time of maximum heave near the crown, springline and invert. Figures 12 and 13 show that the lateral and vertical displacements, respectively, decrease rapidly with distance from the tunnel centreline.

The development of the surface initial heave and final settlement (after consolidation) profiles are drawn in Figure 14. The surface heaves up to 0.88 cm above the tunnel vertical center axis and settles down to 2·89 cm. The observed final settlements are quite close to the predicted values.

The predicted initial heave and final settlement distributions with depth along the vertical centre axis with depth are presented in Figure 15. It can be seen that a large portion of the displacement occurs within 2 m distance above the tunnel crown.

The predicted and measured surface settlements above the tunnel centre axis with time are presented in Figure 16. Good agreement can be seen between the predicted and measured settlements. The surface initially heaves up to 0.88 cm and settles down rapidly to $-1{\cdot}96$ cm during the closure of the tail gap. During the liner erection a little heave occurs due to the fact that an uplift force results from the liner weight and the remaining equivalent nodal tractions. Following that, the surface settles with time to $-2{\cdot}89$ cm due to the dissipation of the excess pore pressure that was developed in the Recent Bay Mud layer during the early stages of the tunneling process. Figure 17 presents the predicted vertical displacements at the tunnel crown and invert with time. During the heaving stage, the crown heaves up while the invert settle down. This behaviour is reversed during the closure of the gap. After that, both the crown and invert almost certain amount of displacement with time.

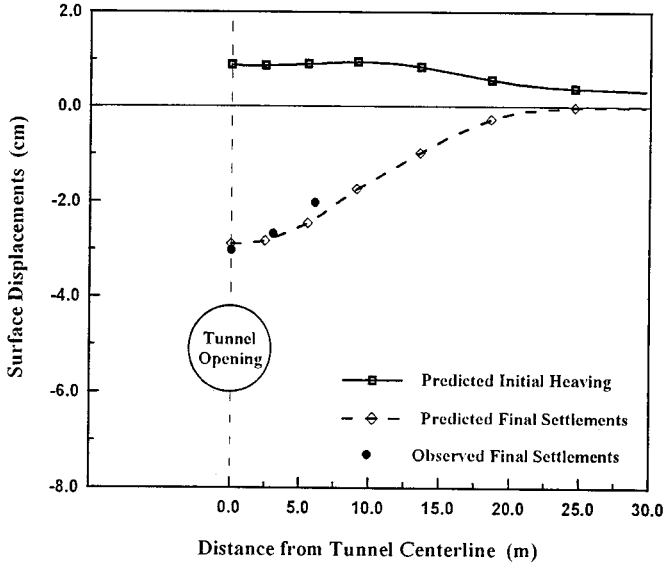

Figure 14. Predicted and observed distribution of surface displacements

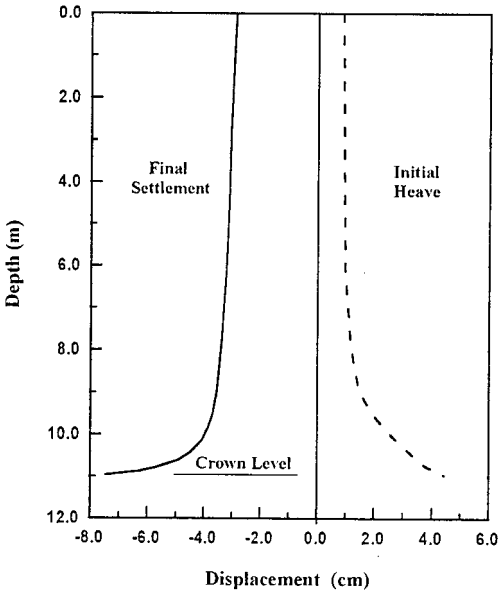

Figure 15. Predicted vertical displacements along the vertical center axis with depth

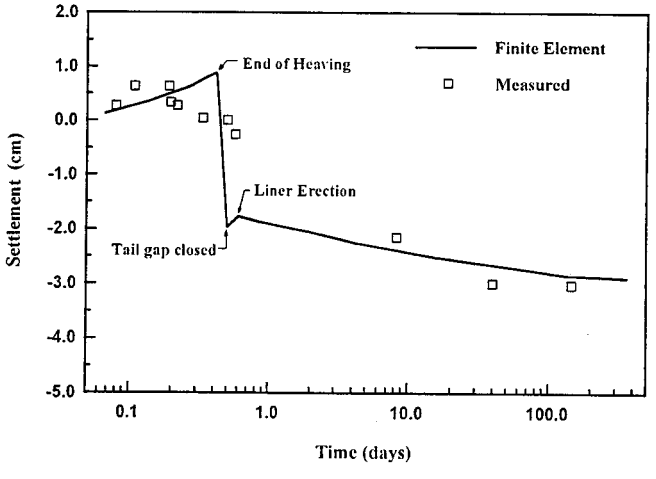

Figure 16. Centreline surface settlement with time

5.4. Excess pore pressure distribution

The calculated contours of the excess pore pressure for the Recent Bay Mud are presented in Figures 18(a) and 18(b) at the maximum heave and after the closure of the tail gap, respectively.

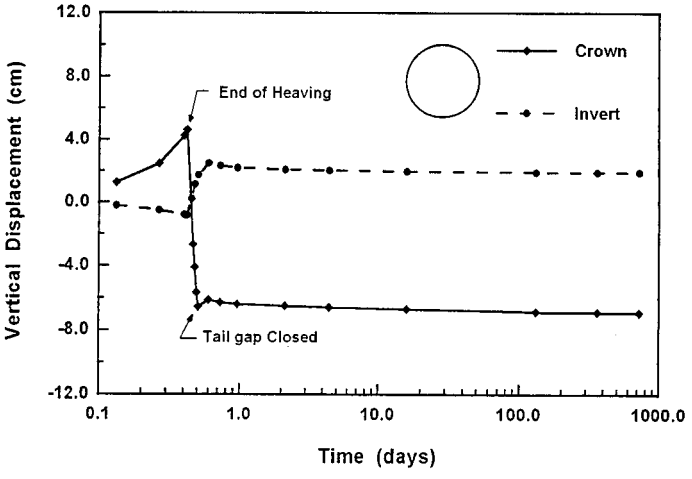

Figure 17. Crown and invert displacements with time

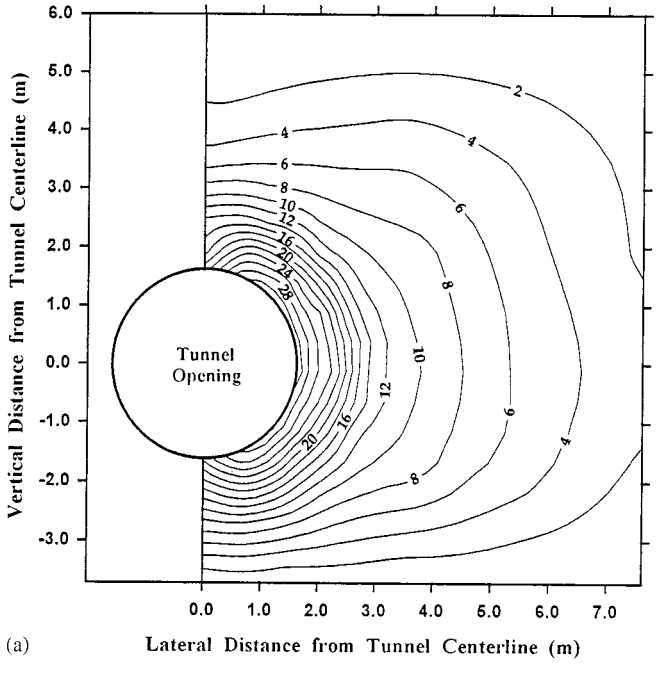

(a)

Figure 18(a). Contours of excess pore pressure at maximum heave (kPa).

The excess pore pressure after heaving varies from about 20 kPa near the tunnel crown and invert to about 30 kPa near and above the tunnel springline. After the gap closure, this excess pore pressure reduces to about 20 kPa near the tunnel springline and a negative pore pressure of up to −10 kPa develops around the tunnel crown and invert. The dissipation of this excess pore

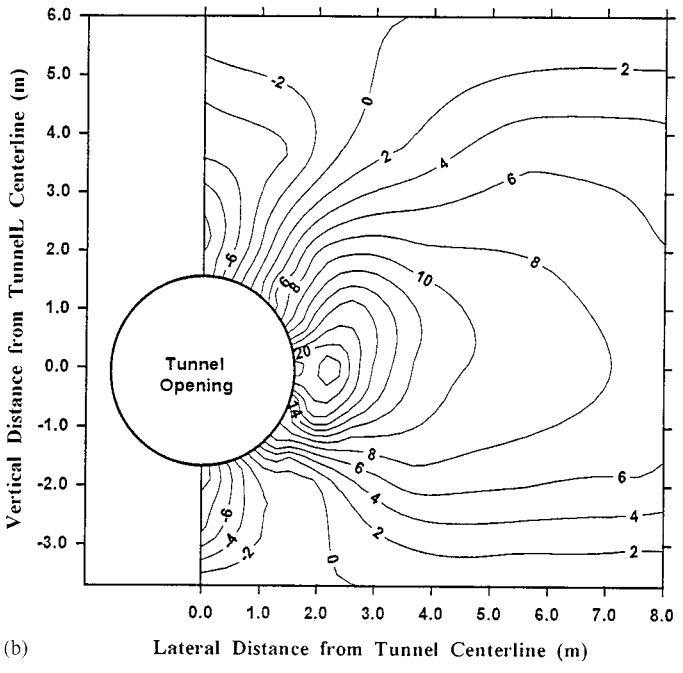

(b)

Figure 18(b). Contours of excess pore pressure after tail gap closed.

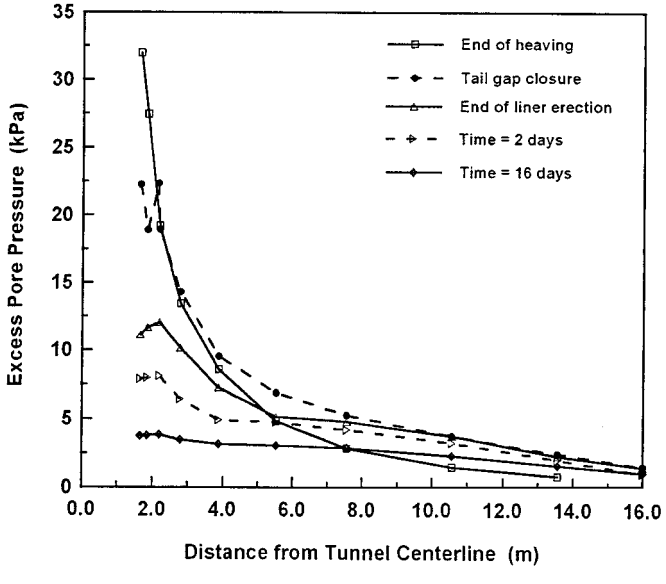

Figure 19. Transverse distribution of the excess pore pressure with distance from tunnel centreline

pressure causes the long-term deformation (consolidation) of the Recent Bay Mud. The transverse distribution of excess pore pressure at different times are presented in Figure 19. Most of the excess pore pressure lies within a 5 m distance from the tunnel centreline.

6. CONCLUSION

An elasto-plastic two-dimensional finite element analysis that is based on the coupled theory of mixtures for inelastic porous media for finite deformation is used in this work. A two-dimensional computational model is developed to simulate the Earth Pressure Balance (EPB) tunneling process in cohesive soils. This model has been used to analyse the N-2 tunnel project constructed in 1981 in San Francisco. Based on this analysis, a number of conclusions may be drawn from the comparisons between the predicted and field measurements.

The developed two-dimensional model of the combined 'longitudinal-transverse' sections is capable of simulating the continuous advance of the EPB shield and incorporating the 3-D deformation caused ahead and around the EPB shield face. This model is also capable of predicting the short term and long term soil deformations caused by the tunneling process.

The predicted longitudinal and lateral displacement profiles are in reasonable agreement with the observed field displacements. Reasonable good agreement is also obtained between the predicted and observed lateral displacements distributions at the maximum heaving.

The distribution of the predicted surface final settlement (after consolidation) agrees well with the observed field measurements. The calculated centerline surface settlement with time compares reasonably well with field measurements.

A positive pore pressure is developed around the tunnel opening during heaving. However, after the tail gap closure, a negative pore pressure develops near the tunnel crown and invert, while a positive pore pressure remains close to the tunnel springline. The dissipation of this excess pore pressure is responsible for the long term (consolidation) settlement.

ACKNOWLEDGEMENTS

This research was supported by the National Science Foundation under grant MSS-9312707. The authors wish to acknowledge the support and encouragement of Dr. Priscilla P. Nelson, Program Director of G3S/CMS, Directorate of Engineering, NSF.

REFERENCES

1. G. Z. Voyiadjis and M. Y. Abu-Farsakh, 'Coupled theory of mixtures for clayey soils', *Comput. Geotech.*, **20**(3/4), 195–222 (1997).
2. S. Babenderede, 'Tunnelling machines in soft ground: a comparison of slurry and EPB shield systems', *Tunneling Underground Space Technol.*, **6** (2), 169–174 (1991).
3. R. B. Peck, 'Deep excavation and tunneling in soft ground', *state-of-the-art Report, Proc. 7th Int. Conf. on Soil Mechanics and Foundation Engng*, Mexico City, 1969, pp. 225–290.
4. K. M. Lee, R. K. Rowe and K. Y. Lo, 'Subsidence owing to tunneling. I. estimating the gap parameter', *Can. Geotech. J.*, **29,** 929–940 (1992).
5. M. C. Ng, K. Y. Lo and R. K. Rowe, 'Analysis of field performance — the Thunder Bay Tunnel', *Can. Geotech. J.*, **23,** 30–50 (1986).
6. R. K. Rowe and G. J. Kack, 'A theoretical examination of settlement induced by tunneling: four case histories', *Can. Geotech. J.*, **20,** 299–314 (1993).
7. R. K. Rowe, K. Y. Lo and G. J. Kack, 'A method of estimating surface settlement above tunnel construction in soft ground', *Can. Geotech. J.*, **20,** 11–22 (1983).

8. R. J. Finno and G. W. Clough, 'Evaluation of soil response of EPB shield tunneling', *J. Geotech. Engng*., *ASCE*, **111**(2)**,** 155–173 (1985).
9. R. K. Rowe and K. M. Lee, 'Subsidence owing to tunneling. II. Evaluation of a prediction technique', *Can. Geotech. J*., **29,** 941–954 (1992).
10. K. M. Lee and R. K. Rowe, 'Finite element modeling of the three-dimensional ground deformations due to tunneling in soft cohesive soils: part I — method of analysis', *Comput. Geotech*., **10,** 87–109 (1990a).
11. K. M. Lee and R. K. Rowe, 'Finite element modeling of the three-dimensional ground deformations due to tunneling in soft cohesive soils: part II — results', *Comput. Geotech*., **10,** 111–138 (1990b).
12. K. M. Lee and R. K. Rowe, 'Deformation caused by surface loading and tunneling: the rule of elastic anisotropy', *Geotechnique*, **39**(1)**,** 125–140 (1989a).
13. K. M. Lee and R. K. Rowe, 'Effects of undrained strength anisotropy on surface subsidence induced by the construction of shallow tunnels', *Can. Geotech. J*., **26,** 279–291 (1989b).
14. H. Akagi, 'Computational simulation of shield tunneling in soft ground', *Memoirs of the School of Science and Engineering*, Waseda University, **58,** 1994, pp. 85–119.
15. M. Y. Abu-Farsakh, 'Coupled field equations for saturated soils and its application to piezocone penetration and shield tunneling', *Ph.D. dissertation*, Department of Civil and Environmental Engineering, Louisiana State University, LA, 1997.
16. A. Tezuka, 'Adaptive remeshing process with quadrangular finite elements', *Adv. Eng. Software*, **12,** 185–201 (1992).
17. N. S. Lee and K. J. Bathe, 'Error indicators and adaptive remeshing in large deformation finite element anal.', *Finite Elements Anal. Des*., **6,** 99–139 (1994).
18. G. W. Clough, B. P. Sweeney and R. J. Finno, 'Measured soil response to EPB shield tunneling', *J. Geotech. Engng*., *ASCE*, **109**(2)**,** 131–149 (1983).
19. M. Y. Abu-Farsakh, G. Z. Voyiadjis and M. T. Tumay, 'Numerical analysis of the miniature piezocone penetration tests (PCPT) in cohesive', *Int. J. Numer. Anal. Methods Geomech*., (1998) in press.

